

Polarization instability of solitons in photonic crystal fibers

F. Luan, A. V. Yulin, J. C. Knight, D. V. Skryabin

Centre for Photonics and Photonic Materials, Department of Physics, University of Bath, Bath
BA2 7AY, UK

<http://www.bath.ac.uk/physics/groups/cppm/>

Abstract: We present experimental and numerical results demonstrating the existence of polarization instability of femtosecond solitons in small core photonic crystal fibers. The frequency of the solitons in our setup shifts rapidly with propagation along the dispersion curve due to the Raman effect. This process can cause initially stable solitons to become unstable, or vice versa depending on the parameters.

© 2006 Optical Society of America

OCIS codes: (060.5530) Pulse propagation and solitons; (190.4370) Nonlinear optics, fibers

References and links

1. J. Herrmann, U. Griebner, N. Zhavoronkov, A. Husakou, D. Nickel, J.C. Knight, W.J. Wadsworth, P.St.J. Russell, and G. Korn, "Experimental evidence for supercontinuum generation by fission of higher-order solitons in photonic fibers," *Phys. Rev. Lett.* **88**, 173901 (2002).
2. J. Dudley, X. Gu, L. Xu, M. Kimmel, E. Zeek, P. O'Shea, R. Trebino, S. Coen, and R. Windeler, "Cross-correlation frequency resolved optical gating analysis of broadband continuum generation in photonic crystal fiber: simulations and experiments," *Opt. Express* **10**, 1215-1221 (2002).
3. L.F. Mollenauer, "Nonlinear optics in fibers," *Science* **302**, 996-997 (2003).
4. D.V. Skryabin, F. Luan, J.C. Knight, and P.St.J. Russell, "Soliton self-frequency shift cancellation in photonic crystal fibers," *Science* **301**, 1705-1708 (2003).
5. A. Efimov, A. V. Yulin, D. V. Skryabin, J. C. Knight, N. Joly, F. G. Omenetto, A. J. Taylor, and P. Russell, "Interaction of an optical soliton with a dispersive wave," *Phys. Rev. Lett.* **95**, 213902 (2005).
6. J.R. Salgueiro, Y.S. Kivshar, D.E. Pelinovsky, V. Simon, and H. Michinel, "Spatial vector solitons in nonlinear photonic crystal fibers," *Studies in Appl. Math.* **115**, 157-171 (2005).
7. M. Hu, C. Wang, Y. Song, Y. Li, L. Chai, E. Serebryannikov, and A. Zheltikov, "Mode-selective mapping and control of vectorial nonlinear-optical processes in multimode photonic-crystal fibers," *Opt. Express* **14**, 1189-1198 (2006).
8. F. Biancalana and D.V. Skryabin, "Vector modulational instabilities in ultra-small core optical fibres," *J. Opt. A* **6**, 301-306 (2004).
9. F. Lu, Q. Lin, W. H. Knox, and G. P. Agrawal, "Vector Soliton Fission," *Phys. Rev. Lett.* **93**, 183901 (2004).
10. K. Blow, N. Doran, and D. Wood, "Polarization instabilities for solitons in birefringent fibers," *Opt. Lett.* **12**, 202-204 (1987).
11. N. Akhmediev, A. Buryak, J. Soto-Crespo, and D. Andersen, "Phase-locked stationary soliton states in birefringent nonlinear optical fibers," *J. Opt. Soc. Am. B* **12**, 434-439 (1995).
12. D. Hutchings and J. Arnold, "Polarization stability of solitons in birefringent optical fibers," *J. Opt. Soc. Am. B* **16**, 513-518 (1999).
13. D. Mihalache, D. Mazilu, and L.-C. Crasovan, "Linear stability analysis of walking vector solitons," *Phys. Rev. E* **60**, 007504 (1999).
14. Y. Barad and Y. Silberberg, "Polarization evolution and polarization instability of solitons in a birefringent optical fiber," *Phys. Rev. Lett.* **78**, 003290 (1997).
15. R. Malendevich, L. Friedrich, G. Stegeman, J. Soto-Crespo, N. Akhmediev, and J. Aitchison, "Radiation-related polarization instability of Kerr spatial vector solitons," *J. Opt. Soc. Am. B* **19**, 695-702 (2002).
16. J.C. Knight, J. Arriaga, T.A. Birks, A. Ortigosa-Blanch, W.J. Wadsworth, and P.S. Russell, "Anomalous dispersion in photonic crystal fiber," *IEEE Photon. Technol. Lett.* **12**, 807-809 (2000).

Photonic crystal fibers (PCFs) have opened up new prospects in studies of many nonlinear optical effects and, amongst other things, stimulated renewed interest in the physics of fiber solitons, see, e.g., [1, 2, 3, 4, 5]. The interplay between polarization and nonlinear effects is often important in PCFs and it has received substantial attention recently, see, e.g., [5, 6, 7, 8] and the related work on supercontinuum generation in tapered fibers [9]. In this paper we present results confirming the existence of polarization instability (PI) of Raman shifted solitons in strongly nonlinear PCFs. PI happens in a birefringent medium when the soliton power exceeds some critical value, so that the linear birefringence is compensated by the nonlinear [10, 11, 12, 13]. For the self-focusing nonlinearity it leads to instability of the scalar soliton polarized along the principal axis having smaller refractive index (fast-wave instability). In general, numerous theoretical studies of the soliton instabilities have been accompanied by a relatively small number of experimental verifications. PI is one of the examples which has been tested experimentally for solitons in telecom fibers [14] and for spatial solitons in planar waveguides [15]. An important and distinct feature of PI of the femtosecond solitons in PCFs is that it is accompanied by the strong soliton self-frequency shift. This generally makes some parts of the fiber length stable for soliton propagation and some others unstable depending on how dispersive properties of the fiber vary with the wavelength of the soliton as it is pulled towards lower frequencies by intrapulse Raman scattering.

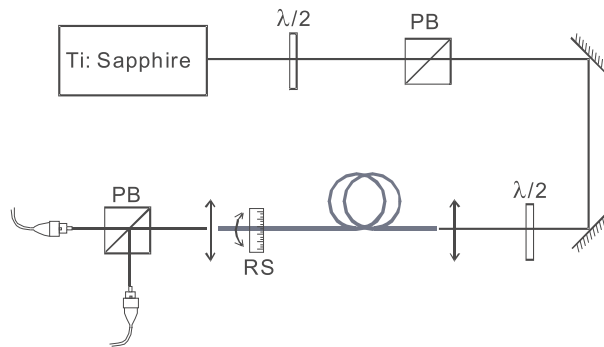


Fig. 1. The experimental setup. 86MHz, 200fs pulses from a Ti:Sapphire laser pass through an attenuator which consists of a half-waveplate and a polarising beam-splitter (PB), then through another half-waveplate to align with the axis of the PCF before coupling into the PCF. The output end of the PCF is mounted onto a rotational stage (RS) to align its axis with the output polarising beam-splitter, enabling independent and simultaneous analysis of the two polarization channels.

Our experimental setup is shown in Fig. 1. The fiber used for our experiments is a small-core (diameter = $0.8\mu\text{m}$) PCF, similar to the one used in Ref. [4]. The group index and group-velocity dispersion (GVD) of the fundamental mode along the two orthogonal fiber axes were measured using a low coherence interferometric method, and the results are shown in Fig. 2. A general feature of small-core PCFs is that the large anomalous waveguide dispersion shifts the zero-GVD wavelength to shorter wavelengths when compared to bulk silica [16], and creates a second zero-GVD wavelength on the long wavelength side. Consequently, the GVD is anomalous only over a finite interval between the two zero-crossings. The soliton dynamics described below occur in the spectral proximity of the second zero GVD point at $\lambda = 1200\text{nm}$. The bire-

fringe of PCFs with hexagonal cladding is non-zero as a consequence of small structural imperfections and the strong waveguiding. We denote the axis with higher (lower) group index at 800nm as s-axis (f-axis). The group index is the ratio of the vacuum light speed to the group velocity of the fiber mode.

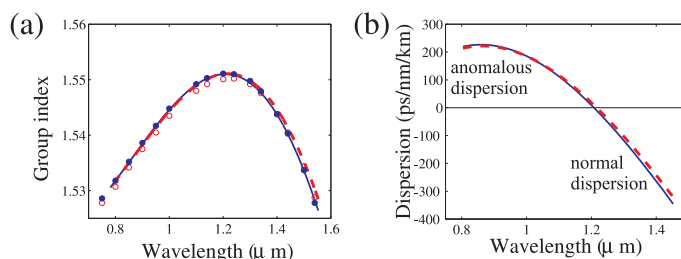


Fig. 2. (a) Group index of the orthogonally polarized modes. Dashed line and open circles correspond to the fast axis and the full line and full circles to the slow axis. Circles mark the experimental measurements, while the lines correspond to the group index used in numerical modelling. (b) Group velocity dispersion (GVD) calculated from the group index. Dashed/full line corresponds to the fast/slow axis.

To explore the possibility of nonlinear coupling between the two polarization axes of our fiber, we set up the following experiment. At the input of the PCF, the polarisation of the pump pulses from a mode-locked Titanium:Sapphire laser (pulse length 200fs; wavelength 790nm; repetition rate 86MHz) is rotated by a half wave-plate and then coupled into the fiber via a high-power aspherical lens. The output end of the 2 meter PCF was mounted in a rotating chuck to align the fiber axis with a polarizing beamsplitter, so that we could analyze the light from the two axes of the fiber independently. The separated channels were then collected by focusing into two multi-mode fibers. The polarization extinction ratio of the laser source and the fiber output was measured to be 30dB and 13dB (in the linear transmission regime) respectively. The difference is partly due to polarization crosstalk in the high-power coupling lens.

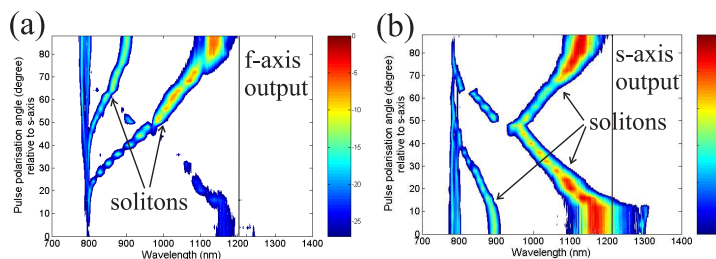


Fig. 3. In this experiment, the input pulse energy was fixed at about 30pJ. The electric vector was rotated through 90 degrees in steps of 4 degrees using the waveplate. At each step, the output spectrum was independently measured for each polarization state. The left (right) plot shows how the spectrum from f-axis (s-axis) evolved during this process. The group velocity dispersion is anomalous to the left of the vertical lines in (a) and (b) and normal to the right.

First, we kept the pulse energy at the input fixed at 30pJ and rotated the input polarisation axis from the s-axis to the f-axis in 4-degree steps. At each step, the spectrum from each axis of the fibre was recorded. Figure 3(a) shows the spectrum recorded from the f-axis output and Fig. 3(b) shows the recorded spectrum from the s-axis output. In the absence of nonlinear

polarisation switching, when the pump pulse energy is higher than the fundamental soliton energy, a soliton is formed which undergoes a soliton self-frequency shift due to the Raman response of the silica. This shift is particularly strong in small core highly nonlinear fibers [17]. As the soliton red-shifts down the GVD curve (Fig. 2) it approaches the longer zero-dispersion wavelength, causing strong resonant radiation towards the long-wavelength side. One effect of this is to introduce spectral recoil, cancelling the soliton shift and stabilising the wavelength [4]. If there were no nonlinear coupling between the fiber axes, then we would expect that both Fig. 3(a) and Fig. 3(b) should have similar patterns, i.e. when the polarization of input pulses are parallel to the fiber axes, the transmitted soliton of that axis has the biggest Raman-shift. This is because all the input energy axis couples to one polarization axis forming the most intense and shortest soliton experiencing largest Raman shift. As the polarization of an input pulse is rotated away from that axis, the total energy is divided between the two axes resulting in weaker Raman shifts. This scenario is clearly seen in Fig. 3(a). 90 degrees angle corresponds to 100% coupling to the fast axis and therefore transmitted soliton spectra is maximally red shifted. As we tune the angle from 90 degrees towards zero, we observe that the Raman shift is also gradually reduces. Spectral evolution observed in the slow axis, see Fig. 3(b), is, however very different. It shows presence of significant amount of energy and large Raman-shifts when the polarization of the input pulses is both parallel (zero degrees) and perpendicular (90 degrees) to the output axis, even though in the absence of nonlinear switching this would be zero at 90 degrees. The difference between Figs. 3a and 3b is compelling evidence of the nonlinearity-mediated energy transfer from the fast axis to the slow, observed when most of the input energy is coupled to the fast axis. It should be emphasized that this behavior was observed in a fiber with a relatively low level of polarization-mode splitting. In other fibers with only slightly different polarization properties, we do not see such switching. Because the cross-polarized power needs to build up from "noise", it is also likely to be sensitive to the level of scattering in a particular fiber length. With the same piece of fiber, we then did a second experiment in which we aligned the

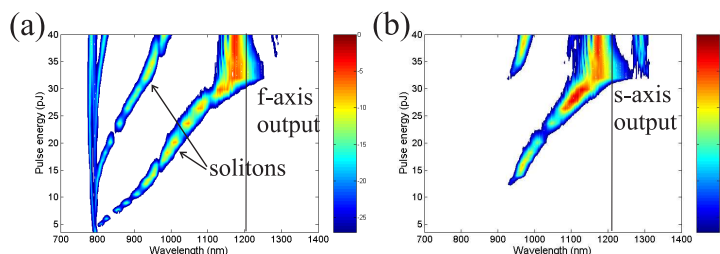


Fig. 4. In this experiment, we fixed the waveplate in front of the PCF and kept the input pulse polarized along the f-axis of the fiber. Then we increased the pulse energy from 3.5pJ to 40pJ in 25 steps. At each step, output spectra for each of the two polarizations were recorded. The left (right) plot shows how the measured spectrum from the f-axis (s-axis) changes during this process. A significant amount of power is coupled from the fast axis into the slow axis under specific conditions. The group velocity dispersion is anomalous to the left of the vertical lines in (a) and (b) and normal to the right.

polarization of the input pulses with the f-axis and recorded the polarized output spectra for different powers (pulse energy ranging from 3.5pJ to 36pJ). Figure 4(a) shows the spectrum from the f-axis and Fig. 4(b) shows the transmission from s-axis. When the incident energy increases above 12pJ there is significant amount of power coupled across to the s-axis. No coupling into the orthogonal polarization was observed when the input pulse was aligned with the s-axis.

To model the observed soliton dynamics we used the coupled generalised nonlinear

Schrodinger (NLS) equations [5]

$$[i\partial_z + D_{x,y}(i\partial_t)]A_{x,y} + \gamma[|A_{x,y}|^2 + \frac{2}{3}|A_{y,x}|^2]A_{x,y} + \frac{\gamma}{3}A_{y,x}^2 A_{x,y}^* + \gamma A_{x,y} \int dt' R(t')I(t-t',z) = 0. \quad (1)$$

Here $I = |A_x|^2 + |A_y|^2$, γ is the nonlinear parameter of the fiber and R is the Raman response function. $D_x(i\partial_t) = \beta_x^{(2)}/2![i\partial_t]^2 + \beta_x^{(3)}/3![i\partial_t]^3 + \dots$, $D_y(i\partial_t) = [\beta_y^{(0)} - \beta_x^{(0)}] + [\beta_y^{(1)} - \beta_x^{(1)}][i\partial_t] + \beta_y^{(2)}/2![i\partial_t]^2 + \beta_y^{(3)}/3![i\partial_t]^3 + \dots$ are the dispersion operators.

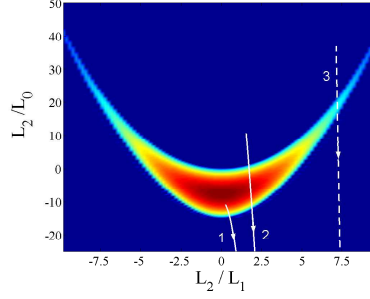


Fig. 5. Plot showing region of PI of the soliton for $q = 20/L_2$. Maximum instability growth rate corresponds to the dark red color and the dark blue background indicates no instability. White lines show several possible ways that the local dispersion parameters experienced by a soliton could change along the fiber length as the soliton was shifted by the Raman effect. Line 1 corresponds to the soliton dynamics shown in Figs. 6,7. Bold lines mark the trajectories when PI was observed in modeling and the dashed ones correspond to the cases when PI did not develop.

First we present results of the stability analysis of the soliton solution $A_x = \sqrt{2q/\gamma}e^{iqz} \text{sech}(t\sqrt{2q/|\beta_x^{(2)}|})$, $A_y = 0$ obtained when we neglect the third and higher-order dispersions and the Raman effect. Assuming that A_y is small we derive the linear equation

$$\left\{ i\partial_z + [\beta_y^{(0)} - \beta_x^{(0)}] + [\beta_y^{(1)} - \beta_x^{(1)}]i\partial_t - \frac{1}{2}\beta_y^{(2)}\partial_t^2 \right\} A_y + \frac{2\gamma}{3}|A_x|^2 A_y + \frac{\gamma}{3}A_x^2 A_y^* = 0. \quad (2)$$

Assuming $A_y = \varepsilon_1(t)e^{\kappa z} + \varepsilon_2^*(t)e^{\kappa^* z}$ we derived an eigenvalue problem for the vector $(\varepsilon_1, \varepsilon_2)^T$ and the full set of the corresponding eigenvalues κ has been found numerically. In Fig. 5 we plot the instability growth rate, i.e. $Re\kappa > 0$, as a function of the inverse birefringence length $L_0 = 1/[\beta_x^{(0)} - \beta_y^{(0)}]$ and of the inverse walk-off length $L_1 = \tau/[\beta_y^{(1)} - \beta_x^{(1)}]$ with both of the latter normalized to the GVD length $L_2 = \tau^2/|\beta_x^{(2)}|$. Here $\tau = 200$ fs is the duration of the input pulse. Regions of strong PI correspond to κ 's with $Im\kappa = 0$. The boundary of the instability range, where one can see small fringes, corresponds to the unstable κ 's with $Im\kappa \neq 0$ [12, 13]. $\beta_{x,y}^{(0)}$ are proportional to the respective refractive indices. Therefore $L_0 > 0$ implies that the x -axis is slower than the y -one. For relatively small $|L_2/L_1|$ the soliton is mostly unstable for $L_0 < 0$ (fast wave instability). The instability of the slow solitons ($L_0 > 0$) existing for larger values of $|L_2/L_1|$ [13] turns out to be irrelevant for interpretation of our experimental results. The plot in Fig. 5 is calculated for $q = 20/L_2$. For weaker solitons (smaller q) the instability region shrinks. It is important to appreciate that as the soliton propagates through the fiber it undergoes the Raman self-frequency shift, therefore all the local dispersion coefficients are changing as it propagates. Several examples of soliton trajectories in the plane $(L_2/L_1, L_2/L_0)$ are shown by white lines in Fig. 5. Even if the soliton traverses through the unstable region, the

propagation length inside this region is always limited and may not be sufficient for the PI to develop to a noticeable level. For example the PI has been observed in numerical modeling for the bold lines in Fig. 5 and has not been seen for the dashed one.

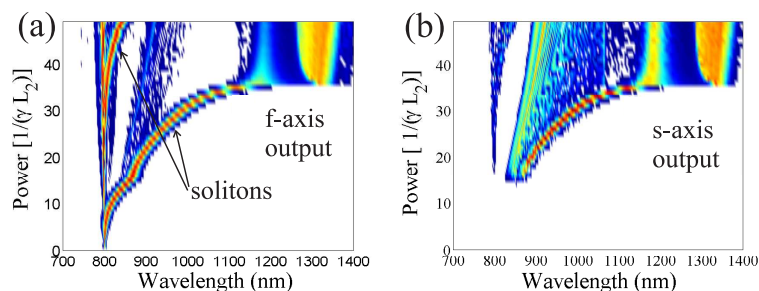


Fig. 6. Transmission spectra of the two polarizations numerically calculated using Eqs. (1). Propagation distance is 2m. Good consistency with experimental measurements in Fig. 4 is evident.

According to our measurements the group velocities of the two polarization components are matched close to $1.4\mu\text{m}$. In order to reach better agreement between our modeling and experimental results we would need to shift this matching point to $1.15\mu\text{m}$, i.e. closer to the pump wavelength, see Fig. 2. It should be noted here that the measurements of the group index are subject to a systematic error related to the vertical shifts of the curves in Fig. 2 by upto ± 0.001 . Results of the direct numerical modeling of Eqs. (1) matching our experimental measurements in Fig. 4 are shown in Fig. 6. For the chosen group index we have the length L_0 varying from -6cm at 800nm (pump wavelength) to -1cm (onset of PI) at 900nm and L_1 varying from 4m at 800nm to 40cm at 900nm . Fig. 7 shows development of the polarization instability in the (z, t) -plane corresponding to the power $25/(\gamma L_2)$ in Fig. 6. One can see only a small part of the full computational window showing essential details of the excitation of the orthogonal polarization and formation of the oscillating vector quasi-soliton. At the initial stage of propagation the input pulse in the left panel is compressed by the nonlinearity. When its amplitude reaches some critical value the orthogonal polarization is excited. The sharp change in the direction of the soliton trajectory occurs because the narrower soliton is more strongly affected by the intrapulse Raman scattering.

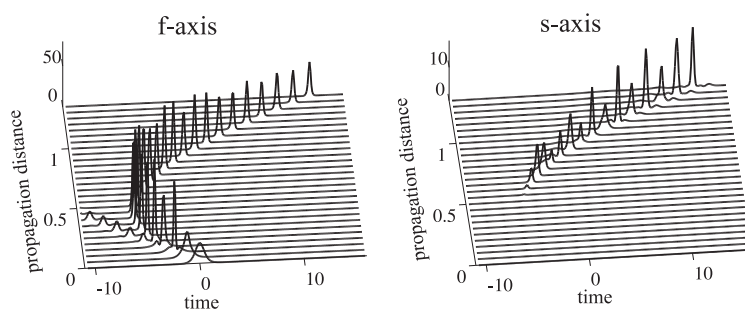


Fig. 7. Polarization instability in the (z, t) -plane, see text for details. Distance, time and intensity are shown in dimensionless units. Physical propagation distance is 40cm . One unit of time is 200fs .

In summary: We have reported the experimental observation and numerical modeling of polarisation instability of the Raman shifted solitons in photonic crystal fibers. This work has

been supported by the Leverhulme Trust.